Biointerface Research in Applied Chemistry
Open-Access Journal (ISSN: 2069-5837)

Article
Volume 16, Issue 1, 2026, 5
https://doi.org/10.33263/BRIAC161.005

Integrative Network Pharmacology and Molecular Modeling Study of Corycavidine in Type 2 Diabetes Mellitus

Ananyaa Srivastava [1], Aakash Jain [2], Jeevan Patra [1,*], Amit K. Keshari [1,*]

[1] Department of Pharmaceutical Chemistry, Amity Institute of Pharmacy, Amity University Uttar Pradesh, Lucknow Campus, Lucknow - 226028, Uttar Pradesh, India; ananyaa.srivastava@s.amity.edu (A.S.);
[2] Department of Pharmacological and Biomolecular Sciences "Rodolfo Paoletti", Università degli Studi di Milano, 20133, Milan, Italy; aakash.jain@studenti.unimi.it (A.J.);
* Correspondence to: jpatra@lko.amity.edu (J.P.); akkeshari@lko.amity.edu / amitkeshari.pharma@gmail.com (A.K.K.);
Received: 6.11.2025; Accepted: 21.01.2026; Published: 15.02.2026

Abstract: Type 2 Diabetes Mellitus (T2DM) is a multifactorial metabolic disorder characterized by chronic hyperglycemia, insulin resistance, and β-cell dysfunction. Although several therapies are available, their long-term effectiveness is limited by adverse effects and poor sustainability. Natural alkaloids offer promising therapeutic potential due to their structural diversity and multitarget activity. Corycavidine, an isoquinoline alkaloid from *Corydalis yanhusuo*, and an intermediate in the isoquinoline biosynthesis pathway, remains largely unexplored for its antidiabetic properties. In this study, we investigated the potential role of Corycavidine in T2DM using an integrative network pharmacology and molecular modeling approach. Compound-target prediction was performed using SwissTargetPrediction, while T2DM-associated genes were obtained from the GeneCards and MalaCards databases. Gene Ontology (GO) and Kyoto Encyclopedia of Genes and Genomes (KEGG) enrichment analyses were conducted using DAVID and ShinyGO, and a Cytoscape-based network was generated with a significance threshold of $p < 0.05$. Protein-protein interactions (PPI) were constructed via String-db, and key hub genes were identified. Molecular docking was performed using MzDOCK with the MMFF94s force field. Top complexes were evaluated for binding stability up to 100 ns using Desmond under the OPLS force field. KEGG analysis revealed significant enrichment in pathways related to insulin signaling, glucose and lipid metabolism, oxidative stress regulation, including PI3K/AKT/mTOR, HIF-1, AMPK, and AGE-RAGE signaling. PPI network analysis identified PIK3R1, PIK3CB, NAMPT, ENPP1, SERPINE1, FABP4, GCK, and ACACB as central hub genes. Docking and MD studies demonstrated strong and stable interaction of Corycavidine with NAMPT (ΔG_{bind} –47.8 kcal/mol) and KDM1A (ΔG_{bind} –63.49 kcal/mol). This study provides the first comprehensive computational insights into the potential antidiabetic mechanisms of Corycavidine, which modulate multiple targets involved in metabolic regulation and insulin sensitivity. Corycavidine emerges as a promising natural scaffold for T2DM therapeutics. Further *in vitro* and *in vivo* studies are necessary to validate these findings.

Keywords: type 2 diabetes mellitus; corycavidine; Corydalis; network pharmacology.

1. Introduction

Type 2 Diabetes Mellitus (T2DM) accounts for nearly 90% of global diabetic cases and is characterized by chronic hyperglycemia, impaired insulin sensitivity [1]. According to the International Diabetes Federation (IDF), the worldwide prevalence of diabetes is projected to reach 578 million by 2023, and 784 million by 2045, highlighting its rapidly increasing public health burden [2]. T2DM is associated with multiple metabolic complications, including diabetic foot, cardiomyopathy, nephropathy, neuropathy, and retinopathy. Current therapeutic strategies primarily target glycemic control, blood pressure, and lipid regulation [3,4]; however, many agents are limited by adverse effects, tolerance development, and suboptimal long-term efficacy [5,6]. Consequently, identifying safer, multitarget therapeutic candidates remains an urgent need for T2DM [7].

Natural products, particularly alkaloids, represent a rich source of structurally diverse bioactive molecules and are used in traditional chinese medicine (TCM) [8]. Traditional Chinese Medicine includes numerous botanical formulations with documented benefits for managing hyperglycemia and metabolic dysfunction [9]. *Corydalis yanhusuo* (*Corydalis rhizoma*), a medicinal plant from the Papaveraceae family, contains several pharmacological properties [10]. Several phytoconstituents are isolated from Corydalis, amongst which alkaloids are the major pharmacologically active ingredients [11-13]. Among these alkaloids, Corycavidine has been an attractive ingredient and a key intermediate in isoquinoline biosynthesis [14]. To date, no studies have evaluated its potential relevance to metabolic regulation, thereby presenting an opportunity to explore its pharmacological utility.

Network pharmacology is an emerging approach to big data analysis in drug research, providing a better understanding of disease mechanisms [15,16]. It provides a holistic view of bioactive components across the diseasome, revealing the interplay among interacting genes and associated pathways [17]. Molecular docking and dynamics simulations validate binding affinity, structural compatibility, and conformational stability at the molecular level. In this study, we aimed to investigate the potential antidiabetic mechanisms of Corycavidine using an integrative computational strategy. This framework may guide future experimental validation and support the identification of novel multitarget scaffolds for diabetes management.

2. Materials and Methods

2.1. Corycavidine target prediction and T2DM gene collections.

Corycavidine's targets were predicted using SwissTargetPrediction (http://www.swisstargetprediction.ch/predict.php). The intrinsic T2DM-associated genes were retrieved from GeneCards (https://www.genecards.org/) and MalaCards (https://www.malacards.org/) databases to ensure high disease specificity. All curated genes were verified, and duplicate genes were removed for further network analysis.

2.2. Commonalities interplaying genes and PPI networks.

The Corycavidine targets and the intrinsic T2DM-associated genes are clustered in two distinct datasets, with no duplicates. The common overlapping genes between these two datasets were obtained using Venny 2.1.0 (https://bioinfogp.cnb.csic.es/tools/venny/). The overlapping genes were considered for subsequent enrichment and network analyses.

Protein-protein interactions (PPI) among the overlapping genes were generated using Stringdb (https://string-db.org/). The Organism was set as '*Homo sapiens*', with a minimum interaction score of 0.400. This score was chosen because it balances false positives and interaction coverage for moderately characterized Corycavidine targets. The TSV files were imported into Cytoscape 3.10.2 (https://cytoscape.org) for topological network evaluation. For the clustering, the Molecular Complex Detection (MCODE) plugin was used to detect highly interconnected clusters. The node score cutoff at 0.2 to remove low-weight or isolated nodes, the K-Core cutoff at 2 to ensure minimum interaction density, and the degree cutoff at 2 were adjusted to avoid over-fragmentation of the network.

2.3. KEGG and GO enrichment analysis.

The predicted genes were imported into the Database for Annotation, Visualization, and Integrated Discovery (DAVID) (https://davidbioinformatics.nih.gov/) platform. The KEGG PATHWAY database (https://www.genome.jp/kegg/pathway.html) was used to validate and annotate the hub genes in the T2DM pathways. The identifier selected as 'GENE_OFFICIAL_SYMBOL' and species characterized as '*Homo sapiens*' to perform Gene Ontology (GO) and Kyoto Encyclopedia of Genes and Genomes (KEGG) enrichment analysis. The GO enrichment screening was performed at a significance cut-off of $p < 0.05$, and the three aspects of biological process (BP), cellular component (CC), and molecular function (MF) were interpreted using R-studio, and ShinyGo v 0.81 (http://bioinformatics.sdstate.edu/go/).

2.4. Protein and ligand preparation.

The selected crystallographic structures for this study were retrieved from the RCSB PDB bank and imported into UCSF Chimera. The non-essential crystallographic species, including heteroatoms, cofactors, and solvent molecules, were removed. The protein structure was examined for missing loops, hydrogen atoms were added to ensure proper protonation at physiological pH 7.4, and the system was minimized to obtain a relaxed, stable conformation.

2.5. Receptor grid production and molecular docking.

MzDOCK is an integrated GUI-based pipeline that computes using the MMFF94s force field, thus providing accurate and reliable docking poses when compared with any standard [18]. The grid was centered on the defined co-crystallized ligand coordinates with a 4.0 Å expansion to generate a three-dimensional grid box. Docking was performed with the default MzDOCK parameters, and molecular interactions were visualized in PyMOL.

2.6. Molecular dynamics simulation and MM-PBSA calculations.

Molecular dynamics simulations of all complexes were performed using the Desmond academic version 2024 to evaluate the structural stability and conformational flexibility. The best-docked conformers were solvated using the single-point-charge extended (SPC-E) explicit water model, truncated in an orthorhombic box extending 10 Å in all directions. The systems were neutralized with 0.15 M NaCl, and energy minimization was performed using the steepest descent algorithm until a gradient threshold of 25 kcal/mol/Å was reached. The non-bonded interaction cut-off distance for coulombic and van der Waals forces was set to 9.0 Å, and long-range electrostatics were treated using the Particle Mesh Ewald (PME) method. A dielectric constant of 1.0 was applied to the system for non-bonded interactions. Each system was

equilibrated under isothermal-isobaric ensemble conditions at 300 K and 1.013 bar using the Nose-Hoover thermostat and the Martyna-Tobias-Klein barostat. The time step was set to 2 fs, and the run was up to 100 ns under the OPLS4 force field.

The absolute binding free energy (ΔG_{bind}) of the highest docked hit was estimated using the molecular mechanics-poisson boltzmann surface area (MM-PBSA) implemented in the g_mmpbsa package [19]. The last 20 ns trajectory of the 100 ns MD simulation was used for free energy calculations, and 500 uniformly sampled snapshots were extracted to ensure statistical stability. Energetic components—including van der Waals, electrostatic, polar solvation, and nonpolar solvation—were reported as mean ± standard deviation, complying with MM-PBSA reporting standards.

3. Results and Discussion

3.1. Identification of Corycavidine and T2DM genes and overlapping targets.

SwissTargetPrediction yielded 89 Corycavidine-associated targets. T2DM disease mining produced 660 high-confidence genes (Figure 1A). The overlapping genes were identified using Venny 2.0.1, which revealed commonalities between the clustered datasets, yielding 24 overlapping targets (Figure 1B).

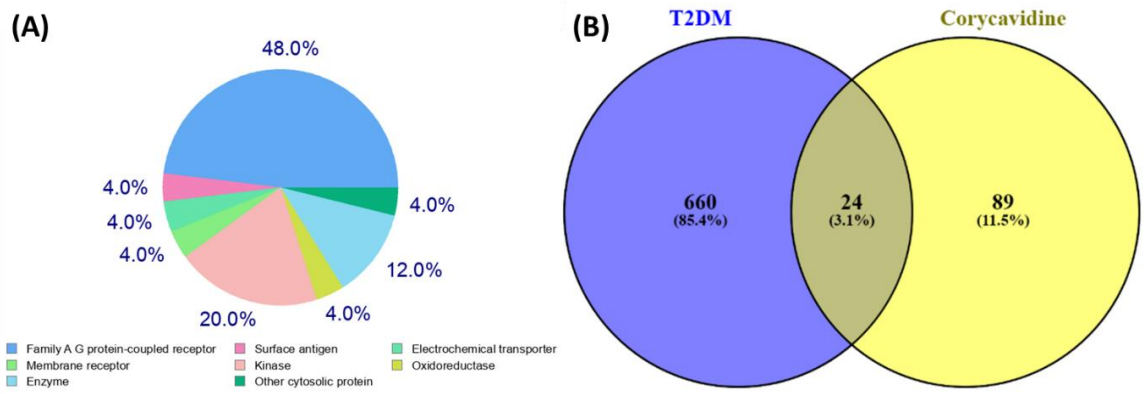

Figure 1. (A) T2DM intrinsic genes; **(B)** Venn diagram for commonalities.

3.2. Functional KEGG and GO enrichment analysis.

The overlapping genes were analyzed through KEGG enrichment using ShinyGo v0.81. The enrichment plot illustrates key signaling and metabolic pathways significantly associated with the common genes, highlighting their biological relevance (Figure 2A and 2B, supplementary Table S1). Among the top enriched pathways, Type II diabetes mellitus (p-value 4.6), central carbon metabolism in cancer (p-value 4.5), and regulation of lipolysis in adipocytes (p-value 4.4) exhibit the highest fold enrichment, indicating a strong link to energy homeostasis and glucose dysregulation. Other notable pathways include renal cell carcinoma (p-value 4.2), prolactin signaling (p-value 4.1), insulin resistance (p-value 4.0), Hypoxia Inducible Factor-1 (HIF-1) signaling (p-value 3.9), and thyroid hormone signaling (p-value 3.8), which collectively point toward an intersection of metabolic and oncogenic processes. Pathways such as Advanced Glycation End products-Receptor Advanced Glycation End products (AGE-RAGE) signaling in diabetic complications (p-value 3.7), Chagas disease (p-value 3.6), insulin signaling (p-value 3.5), glucagon signaling (p-value 3.4), 5' AMP-activated protein kinase (AMPK) signaling (p-value 3.3), cellular senescence (p-value 3.2), and

metabolic pathways (p-value 3.1) further support the involvement of signaling cascades critical in metabolic regulation and diabetic pathology.

Instead of evaluating KEGG terms individually, enriched pathways reveal several coherent biological themes relevant to T2DM. Pathways such as Type II diabetes mellitus, insulin resistance, AMPK signaling, PI3K/AKT, glucagon signaling, and central carbon metabolism converge on insulin responsiveness and glucose homeostasis. These pathways collectively underscore the involvement of the overlapping genes in regulating glucose uptake, hepatic glucose output, β-cell function, and cellular energy balance. Enrichment of AGE–RAGE signaling, HIF-1 signaling, and cellular senescence highlights the interplay between oxidative stress, chronic inflammation, and hypoxic stress—processes central to diabetic complications and β-cell dysfunction. Endocrine pathways such as thyroid hormone signaling and prolactin signaling further point toward metabolic crosstalk between hormonal regulation and glucose metabolism. Cancer-related pathways (e.g., renal cell carcinoma, central carbon metabolism in cancer) appear because metabolic rewiring patterns are shared between cancer and diabetes; this does not suggest oncogenic implications but emphasizes the metabolic adaptability of the enriched genes.

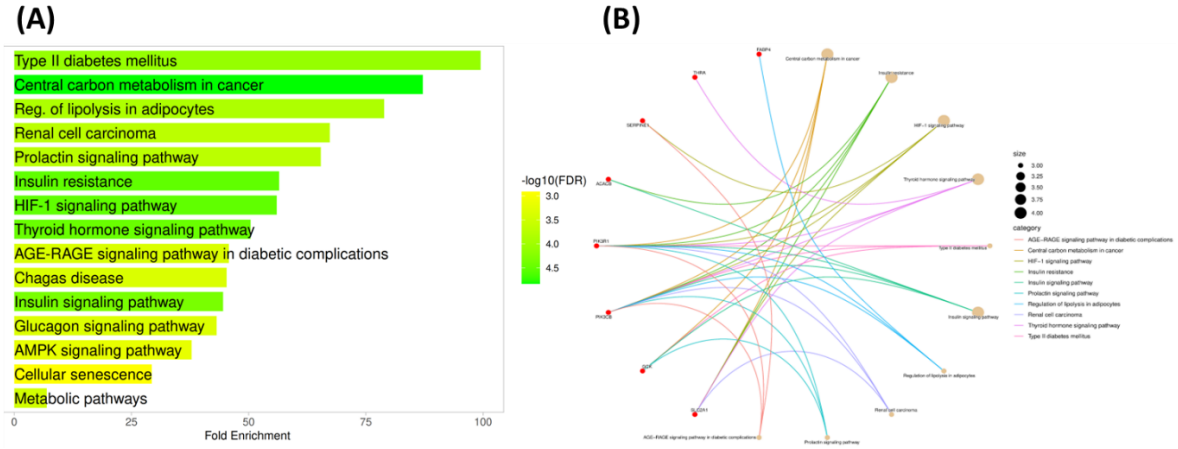

Figure 2. (A) KEGG enrichment analysis. The color gradient from yellow to green corresponds to $-\log_{10}$(FDR) values ranging from 3.0 to 4.5, where deeper green shades denote higher statistical significance; **(B)** KEGG pathway interactions correspond to the number of genes.

The Gene Ontology (GO) enrichment exhibited $p < 0.05$ from the extensive pool of gene annotations. The common genes were imported into the DAVID database with *Homo sapiens* taxonomy, and the GO items for biological processes (BP), cellular components (CC), and molecular functions (MF) were retrieved individually and analyzed (supplementary Table S2). The BP enrichment (Figure 3A), in which glucose import (p-value 4.6), nucleotide and nucleoside metabolic processes (p-value 4.5), and insulin response (p-value 4.4) emerge as key enriched terms, underscores their central roles in energy metabolism and glucose homeostasis. Additional processes, such as positive regulation of cold-induced thermogenesis and transmembrane transport of glucose and monosaccharides, further highlight metabolic adaptation mechanisms. The CC enrichment (Figure 3B) in PIK2 (phosphatidylinositol-3-kinase) complex (p-value 2.7), transferase complex (p-value 2.5), and DNA repair complex (p-value 2.3), suggesting the involvement of the genes in signaling and repair-related molecular assemblies. The MF enrichment (Figure 3C), showing significant terms such as nucleoside-triphosphatase activity (p-value 4.5), insulin receptor binding (p-value 4.3), phosphatidylinositol bisphosphate kinase activity (p-value 4.1), and hormone binding (p-value 3.9), indicates strong links to metabolic regulation and kinase-mediated signal transduction.

The pathway analysis (Figure 3D) revealed central carbon metabolism in cancer (p-value 5.5), insulin resistance (p-value 5.2), HIF-1 signaling (p-value 5.0), thyroid hormone signaling (p-value 4.8), Type II diabetes mellitus (p-value 4.6), and AGE-RAGE signaling in diabetic complications (p-value 4.3) as highly enriched pathways. The cumulative enrichment of all GO items is plotted in Figure 3E with distinct color representations.

GO analysis reinforces the KEGG results by mapping enriched genes to biological processes related to glucose transport, insulin responsiveness, lipid metabolic regulation, and nucleotide biosynthesis, all of which are disrupted in T2DM. Molecular function terms such as insulin receptor binding, kinase regulation, and hormone binding suggest that the targets occupy regulatory positions in metabolic signaling networks. Cellular component enrichment around PI3K complexes and transferase assemblies further supports their involvement in intracellular signaling cascades.

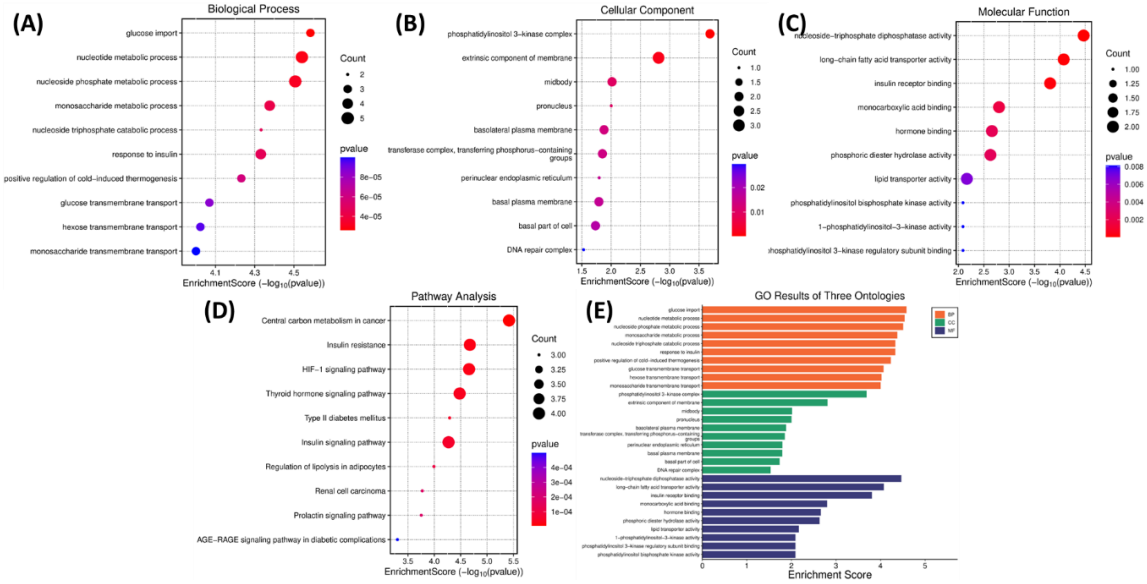

Figure 3. Go enrichment for **(A)** Biological Processes (BP); **(B)** Cellular Components (CC); **(C)** Molecular Functions (MF); **(D)** Pathway analysis; **(E)** cumulative GO items of BP, CC, and MF.

3.3. PPI network analysis and interpretation of network metrics.

The protein-protein interaction (PPI) network of maximal gene count was constructed by connecting Corycavidine, intrinsic disease genes, and pathways. The interactions among the common genes were further analyzed at a medium confidence interval (>0.400) to identify plausible underlying TDM mechanisms (supplementary Table S3). The overlapping genes were submitted to STRING-db to generate an interconnected network with no disconnected nodes. The PPI network was used to identify common genes based on combined scores (supplementary Table S4). The integrative figure overview of the STRING-based PPI network (Figure 4) illustrates functional associations among 13 interconnected nodes implicated in T2DM pathogenesis. Color-coded edges denote various types of interaction evidence emphasizing the coordinated regulation of lipid metabolism, insulin response, and energy homeostasis in T2DM. The network highlights strong interconnections among phosphatidylinositol-3-kinase receptor 1 (PIK3R1), phosphatidylinositol-3-kinase catalytic subunit beta (PIK3CB), ectonucleotide pyrophosphatase phosphodiesterase 1 (ENPP1), nicotinamide phosphoribosyltransferase (NAMPT), glucokinase (GCK), acetyl-CoA carboxylase beta (ACACB), fatty acid binding protein 4 (FABP4), serine protease inhibitor

serpin family E member 1 (SERPINE1), and deoxyuridine triphosphatase (DUT) emerging as a central hub node mediating insulin signaling and glucose homeostasis.

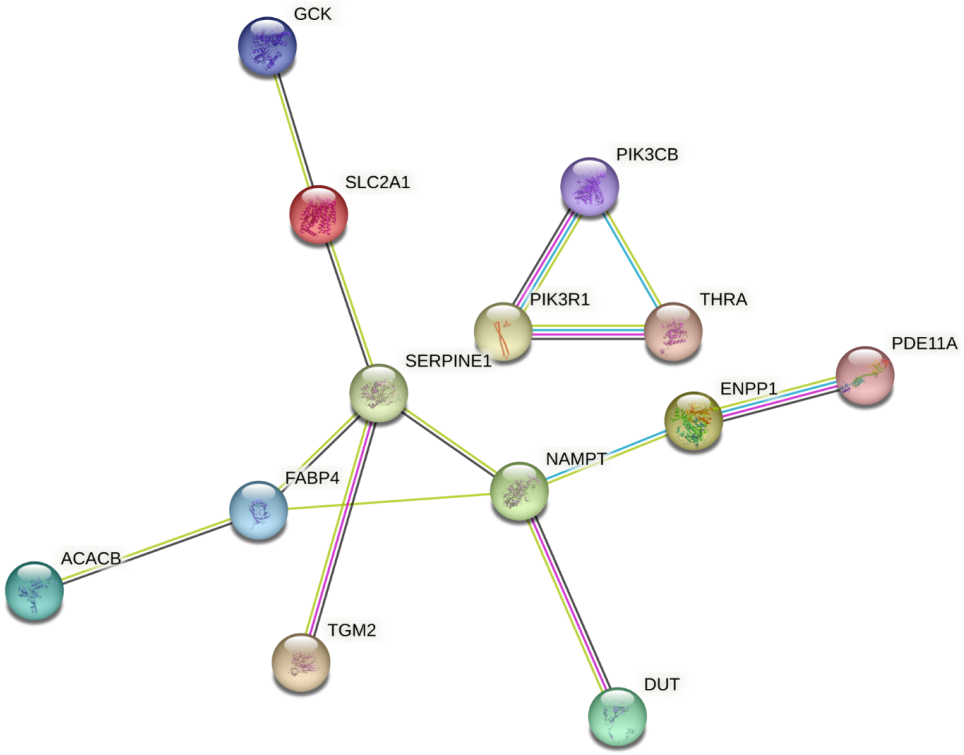

Figure 4. STRING-based protein–protein interaction (PPI) network of the overlapping Corycavidine–T2DM targets.

Simultaneously, the compound–target–disease interaction network, illustrating the linkage between Corycavidine with T2DM, multiple targets, and enriched KEGG pathways. Corycavidine exhibits multitarget engagement with genes such as PIK3CB, GCK, ACACB, phosphodiesterase 11A (PDE11A), DUT, transglutaminase 2 (TGM2), PIK3R1, SERPINE1, NAMPT, and FABP4, which are functionally associated with insulin signaling, glucose metabolism, lipid regulation, and inflammatory response. These targets connect critically with metabolic and signaling pathways, including PI3K/AKT/mTOR, AMPK, AGE-RAGE, HIF-1, and glucagon signaling, reflecting Corycavidine's pleiotropic mechanism of action. The interconnected network supports the KEGG enrichment findings ($-\log_{10}$(FDR) > 2.0), emphasizing statistically significant involvement of pathways regulating insulin resistance, oxidative stress, and energy metabolism. Collectively, the network underscores Corycavidine's therapeutic potential to restore metabolic homeostasis and improve insulin sensitivity through multitarget modulation. Following topology analysis of the constructed PPI network (Figure 5), the network exhibits a density of 0.123, a heterogeneity of 0.342, and a centralization value of 0.164. To evaluate the significance of individual degree-based nodes within this network, we identified eight targets—NAMPT, KDM1A, FABP4, ENPP1, Thyroid hormone receptor alpha (THRA), SERPINE1, PIK3R1, and CNR2 - that interacted equivalently with Corycavidine. The rationale supports the potential implications of these hub genes for T2DM (Table 1).

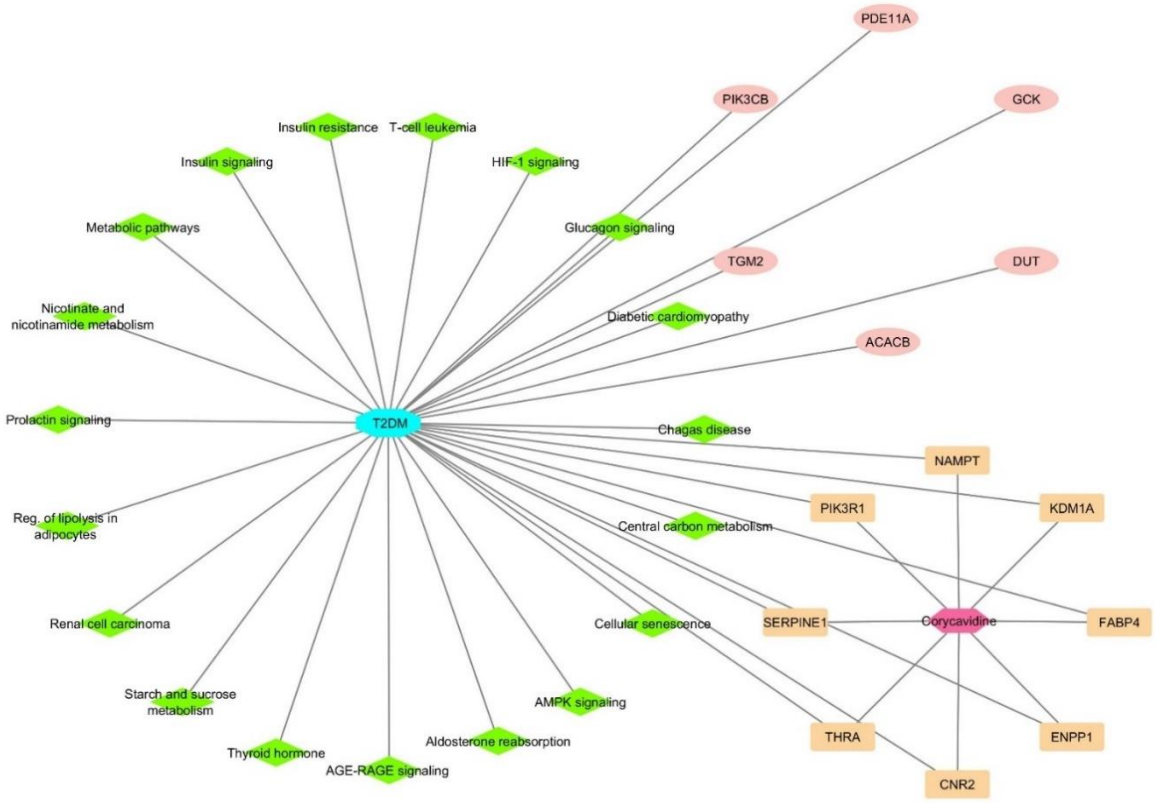

Figure 5. Target pathway between Corycavidine and T2DM. Corycavidine (colored in pink node) linked with T2DM (colored in cyan node), multiple target genes (colored in green, salmon red, and yellow nodes), and enriched KEGG pathways (colored in green diamond nodes).

NAMPT is elevated in T2DM patients and plays a role in the mechanisms of insulin resistance and inflammation. It is the rate-limiting enzyme for NAD^+ synthesis. Targeting NAMPT can improve glucose intolerance and insulin sensitivity [20]. KDM1A regulates gene expression and inflammation, particularly in adipocytes and kidneys. It acts as a histone demethylase, influencing genes involved in obesity-associated inflammation, which can lead to insulin resistance and T2DM [21]. FABP4 elevates serum FABP4 levels and is associated with insulin resistance, a predictor for T2DM [22]. The ENPP1 gene inhibits insulin receptor signaling, leading to insulin resistance [23]. Thyroid dysfunction is common in T2DM and worsens glycemic control and complications. Poorly controlled diabetes affects thyroid hormone levels, leading to subclinical hypothyroidism (high TSH, normal T4), which is frequently seen in T2DM patients [24]. SERPINE1 activates plasminogen activator inhibitor-1 (PAI-1), which is directly linked to T2DM complications [25]. The PIK3R1 gene provides instructions for the 85α regulatory subunit of PI3-kinase in the insulin signaling pathway. Mutations or reduced expression of PIK3R1 can disrupt this signaling, leading to insulin resistance and impairing the regulation of blood sugar levels [26]. CB2 activation for T2DM reduces inflammation, oxidative stress, and cardiac and kidney complications. Stimulating CB2R can improve glucose and lipid metabolism, protect pancreatic β-cells, and alleviate organ damage in diabetes [27].

3.4. Corycavidine interacts with hub genes.

Based on the highest degree nodes and centrality, Corycavidine was assessed against these genes. The PDB for NAMPT, KDM1A, ENPP1, and SERPINE1 genes were retrieved from the RCSB PDB bank (Table 1). The co-crystallized ligands and Corycavidine were

docked into its native binding pocket with identical grid parameters and constraints. The docked complexes achieved a good root-mean-square deviation (RMSD) between the co-crystal and the Corycavidine best-docked pose, indicating a good superposition and confirming the reliability of the docking method. After thorough assessment, the docking scores and binding affinities of Corycavidine against NAMPT and KDM1A were found to have binding free energies, as compared with the co-crystallized ligands of respective genes (Table 2). The molecular interactions in these poses were visualized to identify potential hydrogen and hydrophobic interactions (Figure 6). The absolute binding free energy was estimated using the Molecular Mechanics Poisson-Boltzmann Surface Area (MM-PBSA) method, which accurately estimates the Gibbs free energy (ΔG). The best docked complexes were assessed for MM-PBSA energetic components. The components - van der Waals (ΔG_{vdW}), lipophilicity (ΔG_{lipo}), hydrogen bonding (ΔG_{hbond}), and coulombic (ΔG_{coul}) energies are higher than the co-crystal and are responsible for binding affinity and complex stability (Figure 7).

Table 1. Structural crystallography details of selected genes for considering docking studies.

Sr. No.	Genes	PDB ID	Co-crystallized ligands	Resolution	Ref
1	NAMPT	8Y55	PF403	1.86 Å	[28]
2	KDM1A	6TE1	5-imidazolylthieno-[3,2-*b*]-pyrroles (5-ITP)	3.11 Å	[29]
3	ENPP1	6XKD	4-[(7-methoxyquinolin-4-yl)oxy]-phenyl-sulfuric diamide (MQPSD)	2.73 Å	[30]
4	SERPINE1	7AQG	TM5484	2.27 Å	[31]

Table 2. Dock score, MM-PBSA, and RMSD of the best docked Corycavidine against selected genes compared with the co-crystals of respective genes.

Genes	Co-crystallized ligand			Corycavidine		
	ΔG (kcal/mol)	MM-PBSA (kcal/mol)	RMSD (Å)	ΔG (kcal/mol)	MM-PBSA (kcal/mol)	RMSD (Å)
NAMPT	-6.097	-36.38	0.234	-6.266	-47.80	1.002
KDM1A	-5.174	-55.83	0.212	-5.904	-63.49	0.898
ENPP1	-7.001	-54.43	0.165	-5.542	-54.49	0.911
SERPINE1	-3.173	-47.99	0.142	-3.800	-28.36	1.245

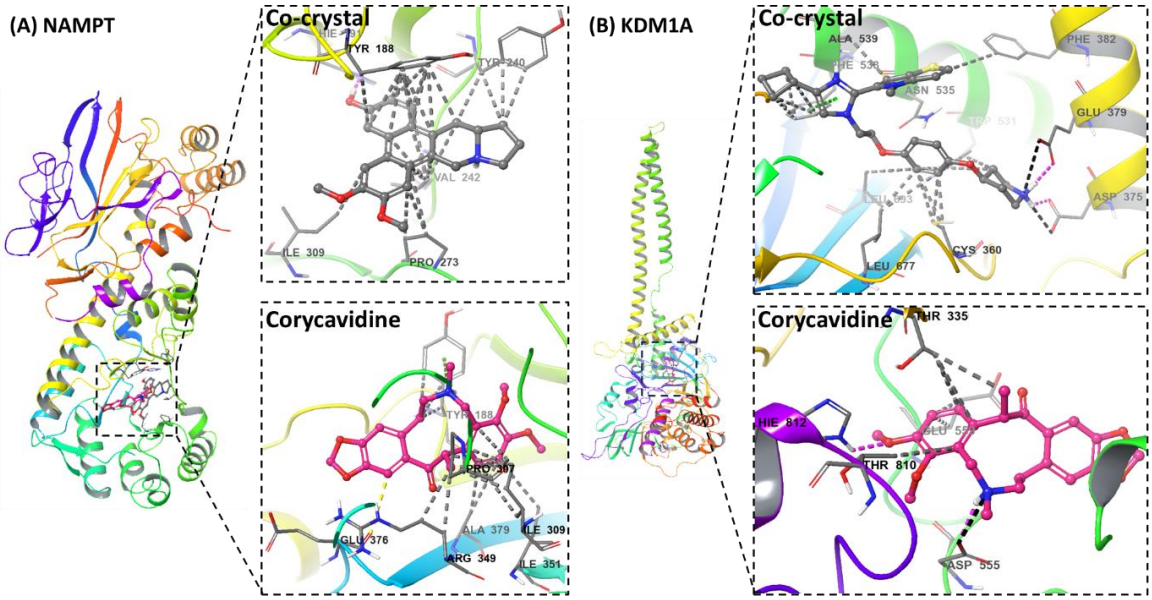

Figure 6. Molecular binding interaction of (**A**) NAMPT complex, and (**B**) KDM1A complexes with respective docked co-crystal (colored in light black), and Corycavidine pose (colored in magenta). The hydrogen bond, aromatic-hydrogen bond, π-π stacking, and hydrophobic are colored in magenta, yellow, green, and grey dashed lines, respectively.

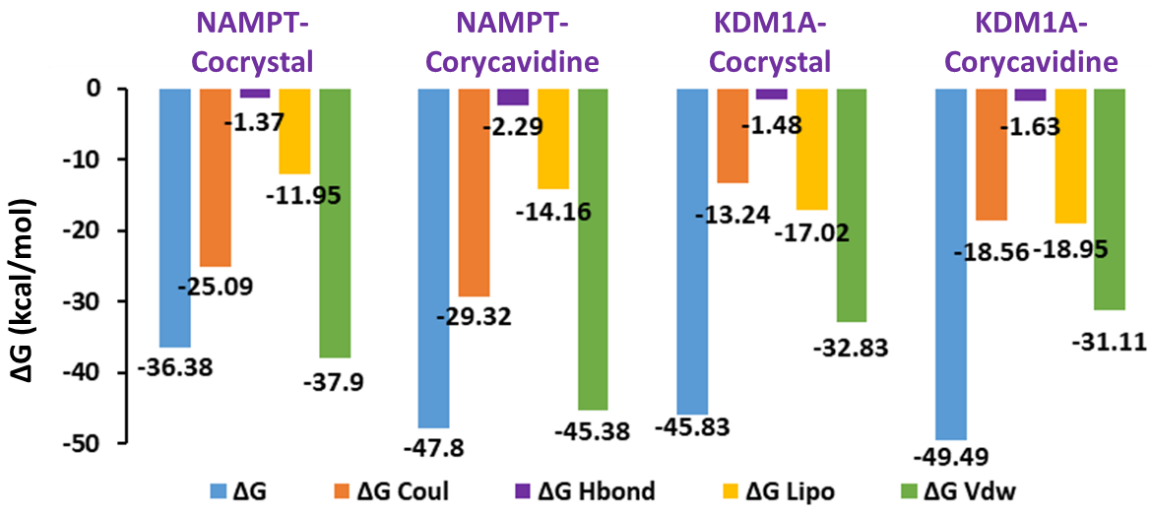

Figure 7. MM-PBSA energetic components estimations of the best docked complexes (NAMPT-Corycavidine and KDM1A-Corycavidine) compared with co-crystals of NAMPT and KDM1A.

3.5. Conformational stability and dynamic behavior analysis.

Molecular dynamics (MD) simulations were conducted to evaluate the conformational stability and dynamic behavior of the best-docked complexes over a 100 ns simulation period. The RMSD reflects the overall stability relative to its initial reference conformer. All complexes exhibited insignificant deviations, indicating successful convergence and equilibration within the binding pocket. The average RMSD for NAMPT-Corycavidine and KDM1A-Corycavidine were 1.21 ± 0.09 Å, and 1.25 ± 0.30 Å, respectively, which were more stable than the reference ligands (respective co-crystals) at 1.7 ± 0.33 Å, and 1.9 ± 0.19 Å, respectively (Figure 8). RMSF analysis was performed to measure residue-level flexibility of the NAMPT-KDM1A complex, co-crystallized with the respective co-crystal and Corycavidine backbone, focusing on α-carbon atoms. Lower RMSF values indicate more rigid and stable regions. The average RMSF for NAMPT-Corycavidine and KDM1A-Corycavidine were 1.01 ± 0.29 Å, and 1.35 ± 0.20 Å, respectively, which were stable as to the co-crystals at 1.1 ± 0.13 Å, and 1.3 ± 0.19 Å, respectively (Figure 9).

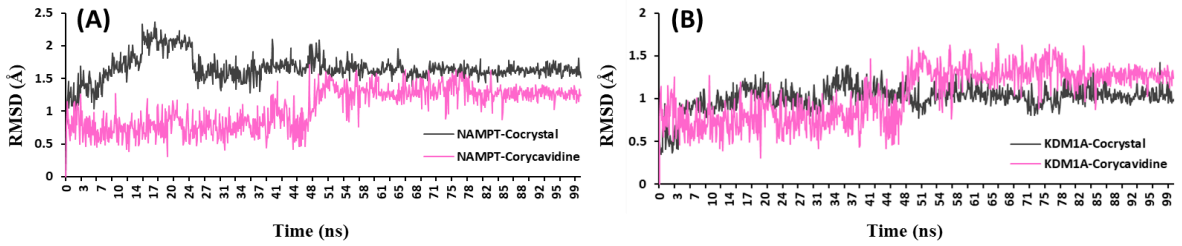

Figure 8. RMSD of best docked NAMPT-Corycavidine and KDM1A-Corycavidine complexes compared with the co-crystals of NAMPT and KDM1A.

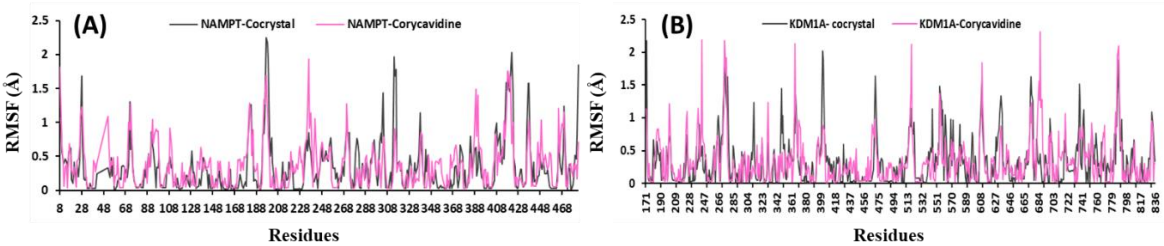

Figure 9. RMSF of the best docked NAMPT-Corycavidine and KDM1A-Corycavidine complexes compared with the co-crystals of NAMPT and KDM1A.

4. Conclusions

This integrative network pharmacology and molecular modeling study provides an initial computational framework for understanding the potential relevance of Corycavidine for T2DM. The overlapping target analysis, GO and KEGG enrichment, docking, MD simulations, and MM-PBSA energy estimations collectively suggest that Corycavidine may interact with multiple proteins implicated in insulin signaling, glucose regulation, lipid metabolism, and oxidative stress. By integrating enrichment and network topology, Corycavidine may influence insulin signaling and glucose homeostasis through interactions with PIK3R1, NAMPT, or ENPP1. It may affect lipid metabolism through FABP4 or ACACB. Epigenetic and stress-response modulation may occur via KDM1A and SERPINE1. The combination of these interactions suggests a potential multitarget metabolic modulation, a hallmark of natural alkaloids. These findings highlight biologically plausible mechanisms through which Corycavidine could influence pathways disrupted in T2DM. However, the study is subject to important limitations inherent to in silico methodologies. The results presented here should be considered hypothesis-generating and provide a mechanistic basis for designing future experiments. Comprehensive in vitro assays, enzyme inhibition studies, cellular models of insulin resistance, and ultimately in vivo evaluations are required to confirm whether Corycavidine can exert meaningful antidiabetic activity and whether its multitarget profile translates into therapeutic benefit.

Author Contributions

Conceptualization, A.S. and J.P.; methodology, J.P. and A.K.K.; software, A.S. and A.J.; validation, J.P.; formal analysis, J.P.; writing—original draft preparation, A.S. and A.J.; writing—review and editing, J.P. and A.K.K.; visualization, J.P.; supervision, J.P. and A.K.K. All authors have read and agreed to the published version of the manuscript.

Institutional Review Board Statement

Not applicable.

Informed Consent Statement

Not applicable.

Data Availability Statement

Data supporting the findings of this study are available upon reasonable request from the corresponding author.

Funding

This research received no external funding.

Acknowledgments

All authors gratefully acknowledged Bioinformatics Resources and Advanced Facility (BRAF) Pune, implemented by the CDAC and supported by the Ministry of Electronics and Information Technology (MeITY) and the Department of Science and Technology (DST), India. The

authors acknowledge Amity Institute of Pharmacy, Amity University Uttar Pradesh, Lucknow Campus, for allowing them to conduct this research work.

Conflicts of Interest

The authors declare no conflict of interest.

Abbreviations

Abbreviation	Definition
Å	Angstrom
BP	Biological Process
CC	Cellular Components
DAVID	Database for Annotation, Visualization, and Integrated Discovery
GO	Gene Ontology
KEGG	Kyoto Encyclopedia Genes and Genomes
MDS	Molecular Dynamics Simulation
MF	Molecular Functions
MM-PBSA	Molecular Mechanics Poisson-Boltzmann Surface Area
PDB	Protein Data Bank
PPI	Protein-Protein Interactions
RMSD	Root Mean Square Deviation
RMSF	Root Mean Square Fluctuation
T2DM	Type II Diabetes Mellitus
TCM	Traditional Chinese Medicine

References

1. Reed, J.; Bain, S.; Kanamarlapudi, V. A Review of Current Trends with Type 2 Diabetes Epidemiology, Aetiology, Pathogenesis, Treatments and Future Perspectives. *Diabetes Metab. Syndr. Obes.* **2021**, *14*, 3567-3602, https://doi.org/10.2147/dmso.S319895.
2. Sun, H.; Saeedi, P.; Karuranga, S.; Pinkepank, M.; Ogurtsova, K.; Duncan, B.B.; Stein, C.; Basit, A.; Chan, J.C.N.; Mbanya, J.C.; Pavkov, M.E.; Ramachandaran, A.; Wild, S.H.; James, S.; Herman, W.H.; Zhang, P.; Bommer, C.; Kuo, S.; Boyko, E.J.; Magliano, D.J. IDF Diabetes Atlas: Global, regional and country-level diabetes prevalence estimates for 2021 and projections for 2045. *Diabetes Res. Clin. Pract.* **2022**, *183*, 109119, https://doi.org/10.1016/j.diabres.2021.109119.
3. American Diabetes, A. 11. Microvascular Complications and Foot Care: Standards of Medical Care in Diabetes—2021. *Diabetes Care* **2020**, *44*, S151-S167, https://doi.org/10.2337/dc21-S011.
4. Nikpour, S.; Mehrdad, N.; Sanjari, M.; Aalaa, M.; Heshmat, R.; Khabaz Mafinejad, M.; Larijani, B.; Nomali, M.; Najafi Ghezeljeh, T. Challenges of Type 2 Diabetes Mellitus Management From the Perspective of Patients: Conventional Content Analysis. *Interact. J. Med. Res.* **2022**, *11*, e41933, https://doi.org/10.2196/41933.
5. Jedlowski, P.M.; Te, C.H.; Segal, R.J.; Fazel, M.T. Cutaneous Adverse Effects of Diabetes Mellitus Medications and Medical Devices: A Review. *Am. J. Clin. Dermatol.* **2019**, *20*, 97-114, https://doi.org/10.1007/s40257-018-0400-7.
6. Cerf, M.E. Beta cell dysfunction and insulin resistance. *Front. Endocrinol.* **2013**, *4*, 37, https://doi.org/10.3389/fendo.2013.00037.
7. Padhi, S.; Nayak, A.K.; Behera, A. Type II diabetes mellitus: a review on recent drug based therapeutics. *Biomed. Pharmacother.* **2020**, *131*, 110708, https://doi.org/10.1016/j.biopha.2020.110708.
8. Atanasov, A.G.; Zotchev, S.B.; Dirsch, V.M.; Orhan, I.E.; Banach, M.; Rollinger, J.M.; Barreca, D.; Weckwerth, W.; Bauer, R.; Bayer, E.A.; Majeed, M.; Bishayee, A.; Bochkov, V.; Bonn, G.K.; Braidy, N.; Bucar, F.; Cifuentes, A.; D'Onofrio, G.; Bodkin, M.; Diederich, M.; Dinkova-Kostova, A.T.; Efferth, T.; El Bairi, K.; Arkells, N.; Fan, T.-P.; Fiebich, B.L.; Freissmuth, M.; Georgiev, M.I.; Gibbons, S.; Godfrey, K.M.; Gruber, C.W.; Heer, J.; Huber, L.A.; Ibanez, E.; Kijjoa, A.; Kiss, A.K.; Lu, A.; Macias, F.A.; Miller, M.J.S.;

Mocan, A.; Müller, R.; Nicoletti, F.; Perry, G.; Pittalà, V.; Rastrelli, L.; Ristow, M.; Russo, G.L.; Silva, A.S.; Schuster, D.; Sheridan, H.; Skalicka-Woźniak, K.; Skaltsounis, L.; Sobarzo-Sánchez, E.; Bredt, D.S.; Stuppner, H.; Sureda, A.; Tzvetkov, N.T.; Vacca, R.A.; Aggarwal, B.B.; Battino, M.; Giampieri, F.; Wink, M.; Wolfender, J.-L.; Xiao, J.; Yeung, A.W.K.; Lizard, G.; Popp, M.A.; Heinrich, M.; Berindan-Neagoe, I.; Stadler, M.; Daglia, M.; Verpoorte, R.; Supuran, C.T.; the International Natural Product Sciences, T. Natural products in drug discovery: advances and opportunities. *Nat. Rev. Drug Discov.* **2021**, *20*, 200-216, https://doi.org/10.1038/s41573-020-00114-z.

9. Lian, F.; Ni, Q.; Shen, Y.; Yang, S.; Piao, C.; Wang, J.; Wei, J.; Duan, J.; Fang, Z.; Lu, H.; Yang, G.; Zhao, L.; Song, J.; Li, Q.; Zheng, Y.; Lyu, Y.; Tong, X. International traditional Chinese medicine guideline for diagnostic and treatment principles of diabetes. *Ann. Palliat. Med.* **2020**, *9*, 2237-2250, https://doi.org/10.21037/apm-19-271.
10. Tian, B.; Tian, M.; Huang, S.-M. Advances in phytochemical and modern pharmacological research of *Rhizoma Corydalis*. *Pharm. Biol.* **2020**, *58*, 265-275, https://doi.org/10.1080/13880209.2020.1741651.
11. Zhang, J.; He, S.; Wang, J.; Wang, C.; Wu, J.; Wang, W.; Li, F.; Li, S.; Zhao, C.; Li, F. A Review of the Traditional Uses, Botany, Phytochemistry, Pharmacology, Pharmacokinetics, and Toxicology of *Corydalis yanhusuo*. *Nat. Prod. Commun.* **2020**, *15*, 1934578X20957752, https://doi.org/10.1177/1934578X20957752.
12. Deng, A.-P.; Zhang, Y.; Zhou, L.; Kang, C.-Z.; Lv, C.-G.; Kang, L.-P.; Nan, T.-G.; Zhan, Z.-L.; Guo, L.-P.; Huang, L.-Q. Systematic review of the alkaloid constituents in several important medicinal plants of the Genus *Corydalis*. *Phytochemistry* **2021**, *183*, 112644, https://doi.org/10.1016/j.phytochem.2020.112644.
13. Liao, D.; Wang, P.; Jia, C.; Sun, P.; Qi, J.; Zhou, L.; Li, X.e. Identification and developmental expression profiling of putative alkaloid biosynthetic genes in *Corydalis yanhusuo* bulbs. *Sci. Rep.* **2016**, *6*, 19460, https://doi.org/10.1038/srep19460.
14. Kamigauchi, M.; Yoshida, M.; Saiki, K.; Sugiura, M.; Nishijo, J.; In, Y.; Ishida, T. Structural/Physicochemical Properties of Corycavidine, a Key Intermetabolite in the Biosynthesis of Isoquinoline Alkaloids, Elucidated by X-Ray Crystallography, Solution Conformation and Thermal Behavior Analyses, and Energy Calculations. *Bull. Chem. Soc. Jpn.* **2000**, *73*, 1233-1241, https://doi.org/10.1246/bcsj.73.1233.
15. Noor, F.; Tahir ul Qamar, M.; Ashfaq, U.A.; Albutti, A.; Alwashmi, A.S.S.; Aljasir, M.A. Network Pharmacology Approach for Medicinal Plants: Review and Assessment. *Pharmaceuticals* **2022**, *15*, 572, https://doi.org/10.3390/ph15050572.
16. Boezio, B.; Audouze, K.; Ducrot, P.; Taboureau, O. Network-based Approaches in Pharmacology. *Mol. Inform.* **2017**, *36*, 1700048, https://doi.org/10.1002/minf.201700048.
17. Ugwor, E.I.; James, A.S.; Amuzat, A.I.; Ezenandu, E.O.; Ugbaja, V.C.; Ugbaja, R.N. Network pharmacology-based elucidation of bioactive compounds in propolis and putative underlying mechanisms against type-2 diabetes mellitus. *Pharmacol. Res. Mod. Chin. Med.* **2022**, *5*, 100183, https://doi.org/10.1016/j.prmcm.2022.100183.
18. Kabier, M.; Gambacorta, N.; Trisciuzzi, D.; Kumar, S.; Nicolotti, O.; Mathew, B. *MzDOCK*: A free ready-to-use GUI-based pipeline for molecular docking simulations. *J. Comput. Chem.* **2024**, *45*, 1980-1986, https://doi.org/10.1002/jcc.27390.
19. Kumari, R.; Kumar, R.; Lynn, A. *g_mmpbsa*—A GROMACS Tool for High-Throughput MM-PBSA Calculations. *J. Chem. Inf. Model.* **2014**, *54*, 1951-1962, https://doi.org/10.1021/ci500020m.
20. Imai, S.-i.; Kiess, W. Therapeutic potential of SIRT1 and NAMPT-mediated NAD biosynthesis in type 2 diabetes. *Front. Biosci.* **2009**, *14*, 2983-2995, https://doi.org/10.2741/3428.
21. Hanzu, F.A.; Musri, M.M.; Sánchez-Herrero, A.; Claret, M.; Esteban, Y.; Kaliman, P.; Gomis, R.; Párrizas, M. Histone demethylase KDM1A represses inflammatory gene expression in preadipocytes. *Obesity* **2013**, *21*, E616-E625, https://doi.org/10.1002/oby.20479.
22. Wang, H.; Cao, J.; Su, J.-b.; Wang, X.-q.; Wang, X.; Zhang, D.-m.; Wang, X.-h. Serum fatty acid-binding protein 4 levels and responses of pancreatic islet β-cells and α-cells in patients with type 2 diabetes. *Diabetol. Metab. Syndr.* **2021**, *13*, 70, https://doi.org/10.1186/s13098-021-00690-z.
23. Bacci, S.; De Cosmo, S.; Prudente, S.; Trischitta, V. *ENPP1* gene, insulin resistance and related clinical outcomes. *Curr. Opin. Clin. Nutr. Metab. Care* **2007**, *10*, 403-409, https://doi.org/10.1097/MCO.0b013e3281e386c9.

24. Kalra, S.; Aggarwal, S.; Khandelwal, D. Thyroid Dysfunction and Type 2 Diabetes Mellitus: Screening Strategies and Implications for Management. *Diabetes Ther.* **2019**, *10*, 2035-2044, https://doi.org/10.1007/s13300-019-00700-4.
25. Fan, Q.; Li, H.; Qin, Y.; Li, L.; Chen, L.; Zhang, L.; Lv, Y.; Liang, D.; Liang, Y.; Long, T.; Xie, L.; Yang, H.; Dong, C.; Zhang, H. Association of *SERPINE1* rs6092 with type 2 diabetes and related metabolic traits in a Chinese population. *Gene* **2018**, *661*, 176-181, https://doi.org/10.1016/j.gene.2018.04.011.
26. Taheri, R.; Mokhtari, Y.; Yousefi, A.-M.; Bashash, D. The PI3K/Akt signaling axis and type 2 diabetes mellitus (T2DM): From mechanistic insights into possible therapeutic targets. *Cell Biol. Int.* **2024**, *48*, 1049-1068, https://doi.org/10.1002/cbin.12189.
27. Coskun, Z.M.; Bolkent, S. Oxidative stress and cannabinoid receptor expression in type-2 diabetic rat pancreas following treatment with Δ^9-THC. *Cell Biochem. Funct.* **2014**, *32*, 612-619, https://doi.org/10.1002/cbf.3058.
28. Li, F.; Zhang, Z.; Shi, Q.; Wang, R.; Ji, M.; Chen, X.; Li, Y.; Liu, Y.; Yu, S. Thermal proteome profiling (TPP) reveals NAMPT as the anti-glioma target of phenanthroindolizidine alkaloid PF403. *Acta Pharm. Sin. B* **2025**, *15*, 2008-2023, https://doi.org/10.1016/j.apsb.2025.02.027.
29. Romussi, A.; Cappa, A.; Vianello, P.; Brambillasca, S.; Cera, M.R.; Dal Zuffo, R.; Fagà, G.; Fattori, R.; Moretti, L.; Trifirò, P.; Villa, M.; Vultaggio, S.; Cecatiello, V.; Pasqualato, S.; Dondio, G.; So, C.W.E.; Minucci, S.; Sartori, L.; Varasi, M.; Mercurio, C. Discovery of Reversible Inhibitors of KDM1A Efficacious in Acute Myeloid Leukemia Models. *ACS Med. Chem. Lett.* **2020**, *11*, 754-759, https://doi.org/10.1021/acsmedchemlett.9b00604.
30. Dennis, M.L.; Newman, J.; Dolezal, O.; Hattarki, M.; Surjadi, R.N.; Nuttall, S.D.; Pham, T.; Nebl, T.; Camerino, M.; Khoo, P.S.; Monahan, B.J.; Peat, T.S. Crystal structures of human ENPP1 in apo and bound forms. *Biol. Crystallogr.* **2020**, *76*, 889-898, https://doi.org/10.1107/s2059798320010505.
31. Sillen, M.; Miyata, T.; Vaughan, D.E.; Strelkov, S.V.; Declerck, P.J. Structural Insight into the Two-Step Mechanism of PAI-1 Inhibition by Small Molecule TM5484. *Int. J. Mol. Sci.* **2021**, *22*, 1482, https://doi.org/10.3390/ijms22031482.

Publisher's Note & Disclaimer

Supplementary Section

Table S1. KEGG and GO enrichment analysis.

Pathways	P-Value	Benjamini	Fold Enrichment	Bonferroni	FDR	Fisher Exact
Central carbon metabolism in cancer	0.000188	0.0267	32.05	0.0264	0.025	0.0000056
Insulin resistance	0.000666	0.0324	20.88	0.0903	0.0303	0.0000308
HIF-1 signaling pathway	0.000684	0.0324	20.69	0.0926	0.0303	0.000032
Thyroid hormone signaling pathway	0.000925	0.0328	18.65	0.123	0.0307	0.000048
Insulin signaling pathway	0.00132	0.0375	16.49	0.171	0.0352	0.0000778
Type II diabetes mellitus	0.00259	0.0613	36.31	0.308	0.0574	0.000068
Regulation of lipolysis in adipocytes	0.00405	0.0822	28.93	0.438	0.077	0.000135
Renal cell carcinoma	0.00566	0.0919	24.38	0.554	0.086	0.000224
Prolactin signaling pathway	0.00582	0.0919	24.04	0.564	0.086	0.000234
AGE-RAGE signaling pathway in diabetic complications	0.0115	0.152	16.90	0.807	0.142	0.00066
Chagas disease	0.0119	0.152	16.57	0.818	0.142	0.000699
Glucagon signaling pathway	0.0128	0.152	15.95	0.841	0.142	0.000781
AMPK signaling pathway	0.0165	0.18	13.99	0.906	0.169	0.00114
Cellular senescence	0.0265	0.269	10.87	0.978	0.252	0.00236
Metabolic pathways	0.03	0.284	2.54	0.987	0.266	0.0114
Diabetic cardiomyopathy	0.0432	0.384	8.33	0.998	0.359	0.00502
Hormone signaling	0.0487	0.39	7.79	0.999	0.366	0.00604
Human T-cell leukemia virus 1 infection	0.0507	0.39	7.62	0.999	0.366	0.00643
Aldosterone-regulated sodium reabsorption	0.0606	0.39	29.94	1.00e+0	0.366	0.00195
Nicotinate and nicotinamide metabolism	0.0606	0.39	29.94	1.00e+0	0.366	0.00195
Starch and sucrose metabolism	0.0637	0.39	28.45	1.00e+0	0.366	0.00216
Carbohydrate digestion and absorption	0.0821	0.39	21.88	1.00e+0	0.366	0.00363
Pyrimidine metabolism	0.0911	0.39	19.62	1.00e+0	0.366	0.0045
Endometrial cancer	0.0926	0.39	19.29	1.00e+0	0.366	0.00466
VEGF signaling pathway	0.0941	0.39	18.96	1.00e+0	0.366	0.00481
Longevity regulating pathway - multiple species	0.0971	0.39	18.35	1.00e+0	0.366	0.00513

Table S2. Gene Ontology enrichment analysis.

Gene Ontology	Gene No.	Group
phosphatidylinositol 3 kinase complex	13	CC
phosphatidylinositol 3 kinase complex class IA	13	CC
extracellular exosome	40	CC
cytosol	67	CC
nucleus	60	CC
insulin receptor substrate binding	13	MF
long chain fatty acid transmembrane transporter activity	13	MF
cyclic AMP phosphodiesterase activity	13	MF
insulin receptor binding	13	MF
nuclear receptor activity	13	MF
ATP binding	33	MF
D glucose import	13	BP
cAMP mediated signaling	13	BP
intracellular glucose homeostasis	13	BP

natural killer cell mediated cytotoxicity	13	BP
phosphatidylinositol phosphate biosynthetic process	13	BP
cellular response to UV	13	BP
cellular response to insulin stimulus	20	BP
positive regulation of cold induced thermogenesis	20	BP
phosphatidylinositol 3 kinase protein kinase B signal transduction	13	BP
cerebral cortex development	13	BP
positive regulation of inflammatory response	13	BP
cytokine mediated signaling pathway	13	BP
immune response	20	BP
negative regulation of DNA templated transcription	20	BP
positive regulation of transcription by RNA polymerase II	27	BP
signal transduction	27	BP

Table S3. Gene Ontology enrichment analysis based on enrichment score.

GOterm	subgroup	Enrichment score
D glucose import	biological process	123.67
cAMP mediated signaling	biological process	89.55
intracellular glucose homeostasis	biological process	89.55
natural killer cell mediated cytotoxicity	biological process	68.34
phosphatidylinositol phosphate biosynthetic process	biological process	63.34
phosphatidylinositol 3 kinase complex	cellular components	462.11
phosphatidylinositol 3 kinase complex class IA	cellular components	308.07
extracellular exosome	cellular components	3.71
cytosol	cellular components	2.43
nucleus	cellular components	2.00
insulin receptor substrate binding	molecular functions	197.47
long chain fatty acid transmembrane transporter activity	molecular functions	160.44
cyclic AMP phosphodiesterase activity	molecular functions	116.68
insulin receptor binding	molecular functions	111.61
nuclear receptor activity	molecular functions	47.54

Table S4. Protein-Protein Interaction pathway analysis.

#node1	node2	node1_string_id	node2_string_id	coexpression	combined_score
ACACB	FABP4	9606.ENSP00000341044	9606.ENSP00000256104	0.119	0.483
DUT	NAMPT	9606.ENSP00000370376	9606.ENSP00000222553	0.049	0.421
ENPP1	NAMPT	9606.ENSP00000498074	9606.ENSP00000222553	0	0.914
ENPP1	PDE11A	9606.ENSP00000498074	9606.ENSP00000286063	0.056	0.914
FABP4	NAMPT	9606.ENSP00000256104	9606.ENSP00000222553	0	0.435
FABP4	SERPINE1	9606.ENSP00000256104	9606.ENSP00000223095	0.062	0.43
FABP4	ACACB	9606.ENSP00000256104	9606.ENSP00000341044	0.119	0.483
GCK	SLC2A1	9606.ENSP00000223366	9606.ENSP00000416293	0.062	0.553
NAMPT	DUT	9606.ENSP00000222553	9606.ENSP00000370376	0.049	0.421
NAMPT	FABP4	9606.ENSP00000222553	9606.ENSP00000256104	0	0.435
NAMPT	SERPINE1	9606.ENSP00000222553	9606.ENSP00000223095	0.068	0.615
NAMPT	ENPP1	9606.ENSP00000222553	9606.ENSP00000498074	0	0.914
PDE11A	ENPP1	9606.ENSP00000286063	9606.ENSP00000498074	0.056	0.914
PIK3CB	THRA	9606.ENSP00000501150	9606.ENSP00000264637	0	0.9
PIK3CB	PIK3R1	9606.ENSP00000501150	9606.ENSP00000428056	0.049	0.999

#node1	node2	node1_string_id	node2_string_id	coexpression	combined_score
PIK3R1	THRA	9606.ENSP00000428056	9606.ENSP00000264637	0.085	0.956
PIK3R1	PIK3CB	9606.ENSP00000428056	9606.ENSP00000501150	0.049	0.999
SERPINE1	NAMPT	9606.ENSP00000223095	9606.ENSP00000222553	0.068	0.615
SERPINE1	TGM2	9606.ENSP00000223095	9606.ENSP00000355330	0.149	0.41
SERPINE1	FABP4	9606.ENSP00000223095	9606.ENSP00000256104	0.062	0.43
SERPINE1	SLC2A1	9606.ENSP00000223095	9606.ENSP00000416293	0.06	0.667
SLC2A1	SERPINE1	9606.ENSP00000416293	9606.ENSP00000223095	0.06	0.667
SLC2A1	GCK	9606.ENSP00000416293	9606.ENSP00000223366	0.062	0.553
TGM2	SERPINE1	9606.ENSP00000355330	9606.ENSP00000223095	0.149	0.41
THRA	PIK3CB	9606.ENSP00000264637	9606.ENSP00000501150	0	0.9
THRA	PIK3R1	9606.ENSP00000264637	9606.ENSP00000428056	0.085	0.956